Bioresource Technology 234 (2017) 77–85

Contents lists available at ScienceDirect

Bioresource Technology

journal homepage: www.elsevier.com/locate/biortech

Removal of antimony (III) and cadmium (II) from aqueous solution using animal manure-derived hydrochars and pyrochars

Lanfang Han [a,b], Haoran Sun [a], Kyoung S. Ro [c], Ke Sun [a,*], Judy A. Libra [d], Baoshan Xing [b]

[a] State Key Laboratory of Water Environment Simulation, School of Environment, Beijing Normal University, Beijing 100875, China
[b] Stockbridge School of Agriculture, University of Massachusetts, Amherst, MA 01003, USA
[c] Coastal Plains Soil, Water, and Plant Research Center, Agricultural Research Service, U.S. Department of Agriculture, 2611 West Lucas Street, Florence, SC 29501, USA
[d] Leibniz Institute for Agricultural Engineering, Max-Eyth-Allee 100, 14469 Potsdam-Bornim, Germany

HIGHLIGHTS

- Adsorption of Sb (III) and Cd (II) by hydrochars and pyrochars was investigated.
- Neutral form of $Sb(OH)_3$ explained the lower Q_{max} for Sb (III).
- Sb (III) mainly interacted with C—O, C=O and OH groups within biochars.
- Hydrochars had lower sorption capacities for Sb (III) and Cd (II) than pyrochars.
- Less negative surface charge and surface polar C led to the low Q_{max} of hydrochars.

GRAPHICAL ABSTRACT

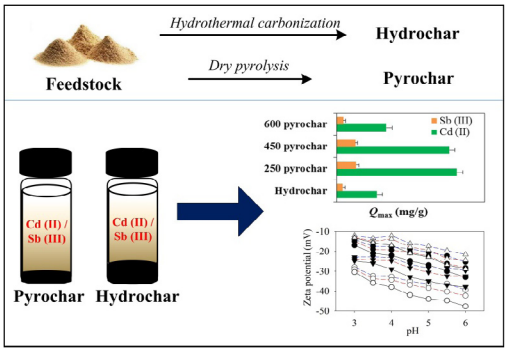

ARTICLE INFO

Article history:
Received 12 December 2016
Received in revised form 23 February 2017
Accepted 26 February 2017
Available online 1 March 2017

Keywords:
Hydrochar
Pyrochar
Cadmium
Antimony
Adsorption

ABSTRACT

In this study, hydrochars and pyrochars prepared from animal manures were characterized and were used to remove Sb (III) and Cd (II) from aqueous solution. Fourier transform infrared spectroscopy (FTIR) analysis revealed the interaction between Cd (II) and C—O and C=O groups within biochars and between Sb (III) and C—O, C=O and OH groups, respectively. Additionally, the lower absolute value of zeta potential of biochar after loading Sb (III) and Cd (II) suggested the occurrence of surface complexation. Existing primarily in the form of $Sb(OH)_3$, the maximum adsorption capacities (Q_{max}) for Sb (III) were lower than those for Cd (II). Due to the lower contents of surface polar functional groups and less negative surface charge, hydrochars exhibited lower Q_{max} for Sb (III) and Cd (II) than pyrochars. However, hydrochars in this study had higher sorption capacities for Cd (II) than most of plant-based pyrochars reported by other literature.

1. Introduction

The contamination of heavy metals in aquatic and soil environments has elicited significant attention due to its vast sources, inherent toxicity and non-degradability (Audry et al., 2004; Järup, 2003; Xu et al., 2014). Elements such as cadmium (Cd), antimony (Sb), chromium (Cr) and nickel (Ni) are classified as heavy metals. Cd and Sb are two of the most toxic heavy metals to human, and Sb (III) is more toxic than Sb (V) (Filella et al., 2002a). It has been reported that once chronically exposed to Cd, human might suffer from diseases such as lung cancer, prostatic proliferative lesions, bone fractures, kidney dysfunction and hypertension (Waalkes, 2000). Sb exposure may result in respiratory

* Corresponding author.
E-mail address: sunke@bnu.edu.cn (K. Sun).

http://dx.doi.org/10.1016/j.biortech.2017.02.130
0960-8524/

irritation, pneumoconiosis, antimony spots on the skin and gastrointestinal symptoms (Sundar and Chakravarty, 2010). Such health risks make studies on the remediation of Cd and Sb contamination high priority.

In recent years, biochars have received considerable interest as effective and environmentally friendly adsorbents for the advanced treatment of heavy metals (Uchimiya et al., 2011; Xu et al., 2013). However, very few sorption studies of Sb on biochars have been reported to date (Filella et al., 2002b; Vithanage et al., 2015) although several investigations have been conducted on the adsorption of Sb onto pure mineral phases (Leuz et al., 2006) and humic substances (Buschmann and Sigg, 2004). Additionally, current research on metal adsorption by the biochars has mostly focused on biochars produced via conventional dry pyrolysis from biomass with low water content (hereafter named as pyrochars) (Audry et al., 2004; Tong et al., 2011; Uchimiya et al., 2010; Xu et al., 2013). For instance, Uchimiya et al. (2010) reported the immobilization of four heavy metal ions (Cu (II), Cd (II), Ni (II) and Pb (II)) by broiler litter-derived pyrochars in water and soil. Tong et al. (2011) investigated the adsorption of Cu (II) by pyrochars generated from three crop straws. By comparison, limited information is available to show the potential environmental applications of biochars produced by alternative thermal conversion technologies such as hydrothermal carbonization (HTC) (Libra et al., 2011). The HTC process usually requires comparatively low temperatures (150–350 °C) and can be applied directly to wet feedstocks such as wet animal manures and algae (Berge et al., 2011; Mumme et al., 2011). It is universally acknowledged that HTC is more energetically favorable than dry pyrolysis processes (Berge et al., 2011; Titirici et al., 2012). HTC occurs by a set of reactions categorized as dehydration, decarboxylation, and recondensation and produces gases (predominantly CO_2), water-soluble organic substances, and carbon (C)-rich solid residues (henceforward referred to as hydrochars) (Titirici et al., 2012). Owing to the dissimilar production process, the structures of hydrochars have been found to differ from those of pyrochars (Cao et al., 2013; Titirici et al., 2012), which would result in their different sorption capacities for organic and inorganic pollutants. One recent study (Han et al., 2016) has found that animal manure-derived 250 °C hydrochars showed higher sorption capacities than pyrochars at 300, 450 and 600 °C for organic pollutants with a wide range of hydrophobicity, suggesting that hydrochar could be utilized as a valuable sorbent for organic pollutants. Yet, very few studies to date have been carried out to directly compare the sorption of heavy metals between hydrochar and pyrochar. It is thus urgent to fill this knowledge gap before designing biochar sorbents to remove both organic and inorganic pollutants from the soils or wastewater.

The objectives of this study were therefore to investigate the effectiveness of hydrochar as sorbents in removing Cd (II) and Sb (III) from wastewater by comparing the differences in sorption capacity between hydrochars and pyrochars. The mechanisms responsible for pollutant removal were elucidated at different pH and using batch sorption isotherms.

2. Materials and methods

2.1. Chemicals

All chemical regents were AR analytical reagent grade. All procedures used the distilled, de-ionized water (DDW) with a resistivity of 18 MΩ·cm (Millipore Corp., Milford, MA). Stock solutions of 1000 mg Cd/L $Cd(NO_3)_2{\cdot}4H_2O$ and 1000 mg Sb/L $KSbC_4H_4O_7$ were prepared with DDW.

2.2. Sorbents

The preparation methods of hydrochars and pyrochars from swine solids and poultry litter were described in detail elsewhere (Spokas et al., 2011). Briefly, hydrochars were prepared by hydrothermally carbonizing swine solids or poultry litter at 250 °C. Dried and ground (less than 2 mm) swine solids and poultry litter were added along with DDW to obtain a slurry of 20% (w/w) solids. This slurry was placed into a 1-L non-stirred T316 stainless steel reactor with an external heater (Parr Instruments, Moline, IL). The operating pressure of the system ranged from 3.4 to 9.0 MPa, representing subcritical conditions. Afterwards, the reactor was cooled to room temperature before the reaction products were filtered and dried at 105 °C. For pyrochars, swine solids and poultry litter with a prior drying treatment were carbonized at 250, 450, 600 °C for 4 h under N_2 condition in a Lindburg electric box furnace equipped with a gas tight retort (Model 51662; Lindburg/MPH, Riverside, MI). The temperature control of the retort system was based on input temperatures allowing for accurate control of pyrolytic exposure temperature. The heating treatment temperatures (HTTs) were raised to the desired values (250, 450 and 600 °C) at a ramp rate of about 8 °C/min. The obtained hydrochars and pyrochars were then washed with 0.1 mg/L HCl followed by DDW until they became neutral, subsequently oven-dried at 105 °C. Then, hydrochars and pyrochars were gently ground, and homogenized to pass through a 0.25 mm sieve. The swine solid- and poultry litter-derived hydrochars were hereafter denoted as HSS250 and HPL250, respectively, and pyrochars were abbreviated and referred as to their individual initial capitals of feedstock source and HTTs (i.e., PSS250, PSS450, PSS600, PPL250, PPL450 and PPL600).

2.3. Sorbent characterization

The bulk C, hydrogen (H), nitrogen (N), and oxygen (O) content of all the biochars were measured by an Elementar Vario ELIII elemental analyzer via complete combustion. The bulk C content is also referred to as the organic carbon (OC) content. Ash content of the biochars was measured by heating samples at 750 °C for 4 h according to the American Society for Testing and Materials (ASTM) D1762-84 (D1762-84, 2007). To get information on surface elemental composition and C-based functionalities, X-ray photoelectron spectra (XPS) of sorbents were recorded with a Kratos Axis Ultra electron spectrometer using monochromated Al Ka source operated at 225 W. Processing of the spectra was accomplished with the Xpspeak41 software. Four components were identified and quantified in the C1s spectra: 284.8 eV (representing C—C and C—H bonds), 286.3 eV (C—O bonds), 287.5 eV (C═O bonds) and 289.0 eV (COOH bonds). The solid-state cross-polarization magic-angle-spinning ^{13}C nuclear magnetic resonance (^{13}C CP-MAS NMR) was done. The NMR running parameters and chemical shift assignments were depicted elsewhere (Ran et al., 2007). The fourier transform infrared (FTIR) spectra of biochars before and after metal sorption were also conducted, and the references for the band assignments were described elsewhere (Qiu et al., 2014). Pore and surface characteristics were examined by gas adsorption using an Autosorb-1 gas analyzer (Quantachrome Instrument Corp., Boynton Beach, FL). The surface topography of hydrochars and pyrochars were investigated using SEM imaging with a Hitachi S4800 scanning microscope (Japan). Surface area ($SA\text{-}CO_2$) and pore size using CO_2 isotherm at 273 K were calculated using nonlocal density functional theory (NLDFT). The surface area using N_2 ($SA\text{-}N_2$) was determined by the Brunauer-Emmett-Teller (BET) equation with multipoint adsorption isotherms of N_2 at 77 K.

2.4. The determination of carbon stability index and stable organic matter yield index (SOMYI)

All studied biochars were oxidized by the hydrogen peroxide (H_2O_2) method (Crombie et al., 2013). Carbon stability is defined as the ratios of OC contents of the biochars after and before the oxidation. Stable organic matter yield index (SOMYI) was determined according to the following equation modified from the study by Masto et al. (2013):

$$SOMYI = Yield/100 \times 1.724 \times OC_{ox} \quad (1)$$

where 1.724 is the factor to convert OC to organic matter, yield (solid yield) is the weight percentage of biochar recovered relative to the total amount of feedstock, and OC_{ox} refers to the OC concentrations of biochars after H_2O_2 oxidation.

2.5. Zeta potential measurements

Zeta potential of each sample at different pH values was measured with Zetasizer 3000 (Malvern Instrument Ltd.). $NaNO_3$ solution (2×10^{-4} M) was used as background electrolyte and NaOH or HNO_3 was used to adjust pH of samples.

2.6. Sorption experiments

A batch equilibration technique was used to obtain the adsorption isotherm of Cd (II) and Sb (III) by sorbents. The test solutions of different concentrations were 0.3–150 mg/L and 0.1–100 mg/L for Cd (II) and Sb (III), respectively. The background solution contained 0.01 M $NaNO_3$ in DDW to maintain a constant ionic strength. The pH of the Cd (II) and Sb (III) solutions was adjusted to 4.5 with either HNO_3 or NaOH to prevent Cd (II) and Sb (III) from being precipitated after addition to the samples. All the sorbents were weighed into 8 mL polypropylene centrifuge tubes, and then the Cd (II) and Sb (III) solutions were added into these tubes and horizontally shaken at 120 rpm for 24 h at room temperature. Preliminary experiments showed that the adsorption equilibrium reached within 24 h. The blanks consisted of sorbate solution without sorbents and sorbents without sorbate. After 24 h, all tubes were centrifuged. The supernatant was withdrawn from each tube and was passed through 0.45 μm filter for the analysis of the inductively coupled plasma optical emissions spectrometer (ICP-AES; SPECTRO Company, Germany). All adsorption experiments were performed in duplicate. The analysis of blank experiments showed that the sorption of each sorbate by the vials was insignificant, and the concentrations of metals which released from hydrochars and pyrochars were all below the detection limits.

The effect of pH on adsorption of Cd (II) and Sb (III) by hydrochars and pyrochars was investigated: 10 mg/L Cd (II) and Sb (III) were placed in empty 8 mL polypropylene centrifuge tubes and a given amount of sorbent was then added to each tube. Suspension pH was adjusted to different values within the range 3.0–6.0 (3.0, 3.5, 4.0, 4.5, 5.0, 5.5 and 6.0). The selection of acidic pH mainly based on the fact that $Cd(OH)_2$ has relatively low solubility, with K_{sp} of 5.27×10^{-15}. At high pH, the metal removal takes place by both adsorption and precipitation when OH— ions formed complexes with Cd (II), which would result in the overestimation of sorption capacity of the studied sorbents. Afterwards, a similar procedure was adopted as described above to obtain the amount of Cd (II) and Sb (III) adsorbed by biochar at different pHs. The solution pH values before and after adsorption equilibrium are listed in Tables S1 and S2.

2.7. Data analysis

The sorption data were fitted to the logarithmic form of Freundlich isotherm model (Eq. (1)), Langmuir (Eq. (2)) and Langmuir-Langmuir (L-L) (Eq. (3)):

$$\log q_e = \log K_F + n \log C_e \quad (2)$$

$$q_e = Q_{max} \times K_L \times C_e/(1 + K_L \times C_e) \quad (3)$$

$$q_e = q_{e,1} + q_{e,2} = Q_{max,1} \times K_{L,1} \times C_e/(1 + K_{L,1} \times C_e) + Q_{max,2} \times K_{L,2} \times C_e/(1 + K_{L,2} \times C_e) \quad (4)$$

where q_e [μg/g] is the equilibrium sorbed concentration; C_e [μg/L] is the equilibrium aqueous concentration; K_F [(μg/g)/(μg/L)^n] is the Freundlich affinity coefficient; and n is the Freundlich exponential coefficient; Q_{max} (mg/g) is the maximum adsorption capacity of the sorbents; K_L (L/mg) is a constant related to binding strength.

The investigated correlations among properties of sorbents as well as their sorption coefficients of all sorbates (Pearson correlation coefficients: p and r values) were obtained from the Pearson correlation analysis by SPSS 16.0 software (SPSS Inc., USA).

3. Results and discussion

3.1. Hydrochars and pyrochars production

The yields of biochar solids from the animal manures in the two thermal processes varied considerably, depending on process conditions (Table 1). While the yields (wt%) for both hydrochars were similar, 55.2% for HSS250, 47.6% for HPL250, the pyrochar yields decreased with HTT: 79.1% for PSS250, 39.9% for PSS450, 36.7% for PSS600, 77.3% for PPL250, 51.0% for PPL450 and 49.7% for PPL600, respectively (Table 1). Obviously, 250 °C pyrochars had higher yields than hydrochars and 450 and 600 °C pyrochars. However, they showed the lower carbon stability indexes (Table 1), indicating that 250 °C pyrochars had a lower proportion of stable OC. Recently, the study by Masto et al. (2013) highlighted that the yields of biochars should be considered when predicting the stable OC fraction of biochars, and they have accordingly proposed the SOMYI index. Further, SOMYI of hydrochars and pyrochars were calculated in this study (Table 1). It was found that the SOMYI values of 450 and 600 °C pyrochars were similar but higher than those of other samples (Table 1), which was different with the results by Masto et al. (2013) where pyrochars at 400 and 500 °C had lower SOMYI than those at 200, 250 and 300 °C.

3.2. Characterization of hydrochars and pyrochars

Adsorption is adsorbent-specific and depends strongly on the physicochemical properties of the adsorbent (Elaigwu et al., 2013; Uchimiya et al., 2010). In this study, the structural characteristics of adsorbents were examined by evaluating their SA and pore size through N_2 and CO_2 sorption isotherms, surface morphology, zeta potential, organic elemental and structural composition.

Both hydrochars (HSS250 and HPL250) presented weakly developed surface area (Table 1), which is common for the other hydrothermally treated materials (Alatalo et al., 2013). For the same feedstock, the pyrochars produced under three HTTs (250, 450 and 600 °C) generally showed higher SA-N_2, SA-CO_2 and smaller pore sizes than hydrochars produced at 250 °C. However, hydrochars or same HTT-produced pyrochars from different feedstocks (swine solids and poultry litter) had the similar SA. Also, SEM images indicated that there were no significant differences in surface morphology between swine solids and poultry litter-derived biochar (Fig. S1). By comparison, surface morphology

Table 1
Yield, bulk and surface elemental compositions and surface area analysis of hydrochars and pyrochars.

Samples	Yield (%)	C (%)	H (%)	N (%)	O (%)	H/C	(O + N)/C	Ash (%)	SA-N_2 (m^2/g)	SA-CO_2 (m^2/g)	Pore size (nm)	Carbon stability index	SOMYI
Bulk elemental composition (elemental analysis)													
HSS250	55.20	54.02	5.69	2.67	12.51	1.26	0.22	25.11	1.87	22.38	0.82	0.40	20.45
PSS250	79.10	50.92	5.55	3.30	20.22	1.31	0.35	20.01	1.20	29.13	0.57	0.29	19.79
PSS450	39.90	42.29	2.38	3.25	10.58	0.68	0.25	41.50	14.25	138.99	0.48	0.74	21.39
PSS600	36.70	44.62	1.37	2.82	7.92	0.37	0.19	43.29	5.51	205.56	0.50	0.79	22.24
HPL250	47.60	39.13	3.06	3.09	8.95	0.94	0.24	45.77	2.77	24.23	0.82	0.52	16.62
PPL250	77.30	40.81	3.93	3.40	25.60	1.15	0.54	26.26	2.99	35.11	0.60	0.33	17.93
PPL450	51.00	37.44	1.79	2.86	10.44	0.58	0.27	47.46	4.76	135.74	0.48	0.77	25.25
PPL600	49.70	38.80	1.10	2.26	8.36	0.34	0.21	49.49	4.20	150.01	0.48	0.82	27.37

	Total C (%)	C—C (%)	C—O (%)	C=O (%)	COOH (%)	O (%)	N (%)	Si (%)	Ca (%)	P (%)	Surface O/C	Surface (O + N)/C
Surface element composition												
HSS250	79.08	87.77	7.42	2.18	2.62	17.04	3.11	0.78	0.33	0.56	0.16	0.20
PSS250	77.74	83.78	10.81	1.80	3.60	19.08	2.69	0.49	0.88	0.93	0.18	0.21
PSS450	64.47	87.57	4.52	4.52	3.39	30.74	3.37	1.42	3.00	3.29	0.36	0.40
PSS600	71.66	83.10	10.33	2.82	3.76	24.46	3.40	0.48	10.02	13.24	0.26	0.30
HPL250	57.26	88.57	5.24	4.29	1.90	30.08	4.77	7.88	4.69	4.73	0.39	0.47
PPL250	54.01	76.70	9.66	11.93	1.70	36.36	7.84	1.80	1.98	2.29	0.50	0.63
PPL450	64.56	85.96	8.77	5.26	4.09	28.99	3.68	2.77	4.33	4.62	0.34	0.39
PPL600	62.42	79.14	9.82	6.13	4.91	31.01	2.27	4.30	8.93	10.12	0.37	0.40

The polarity index ((O + N)/C) of individual samples was calculated from the atomic ratio of (O + N) and C; pore size was obtain via CO_2 adsorption isotherm. Note that SOMYI means the stable organic matter yield index; the capital "H and P" represent hydrochars and pyrochars, respectively; SS and PL mean the biochars obtained from swine solid and poultry litter, respectively; 250, 450 and 600 refer to the heating treatment temperature (°C) of pyrochars.

was HTT-dependent, to some extents. With the increase of HTTs, the surfaces of pyrochars generally became "cleaner", flatter and more inerratic. These data suggested that biochar pyrolysis condition, rather than the feedstock source, played a major role in the SA and surface morphology of biochar.

Table 1 lists the bulk and surface elemental compositions of hydrochars and pyrochars. Similar bulk OC contents of hydrochar and pyrochars from the same feedstock were detected. According to the classification of biochars based on their C content (Lehmann and Joseph, 2015), all the biochar samples belonged to low-C biochars (< 60%). In contrast, the ash contents of all the biochars varied relatively greatly, ranging from 20.01% to 49.49%. The bulk O content of swine solid- and poultry litter-derived biochars followed the sequence: PSS250 (20.22%) > HSS250 (12.51%) > PSS450 (10.58%) > PSS600 (7.92%) and PPL250 (25.60%) > PPL450 (10.44%) > HPL250 (8.95%) > PPL600 (8.36%), respectively. By comparison, the surface O contents changed in a comparatively different pattern. In general, the pyrochars at three HTTs showed more abundant surface O than the corresponding hydrochars (Table 1). Additionally, the abundance of surface oxygen-containing functional group was of interest considering that it plays an important role in the adsorption capacity and the removal mechanism of heavy metals (Alatalo et al., 2013). The bar graph (Fig. 1a) neatly illustrated the generally higher percentage of surface oxygen-containing functional groups (C—O, C=O and COOH) of pyrochars than hydrochars, consistent with the lower zeta potential (due to more negative surface charge) of pyrochars than hydrochars (Fig. 2a and b).

The NMR spectra are illustrated in Fig. S2. Clearly, two hydrochars were dominated by alkyl C (0–45 ppm) although aromatic C (108–148 ppm) also contributed. In contrast, the NMR spectra for pyrochars, especially for pyrochars produced at 450 °C and 600 °C, showed a large contribution from aromatic C (108–148 ppm), and a negligible contribution from paraffinic C (0–45 ppm) and other structural groups (Fig. S2) (Sun et al., 2011). Specific to the polar functional groups, it was noticed that the percentage of methoxyl, carbohydrate, carboxyl and carbonyl C almost reached peak in the 250 °C pyrochars (Table S3), mainly due to the lower decarboxylation and decarbonylation of feedstocks at 250 °C. It has been demonstrated that decarboxylation and decarbonylation extent of biochars generally increased with increasing HTTs (Lehmann and Joseph, 2015).

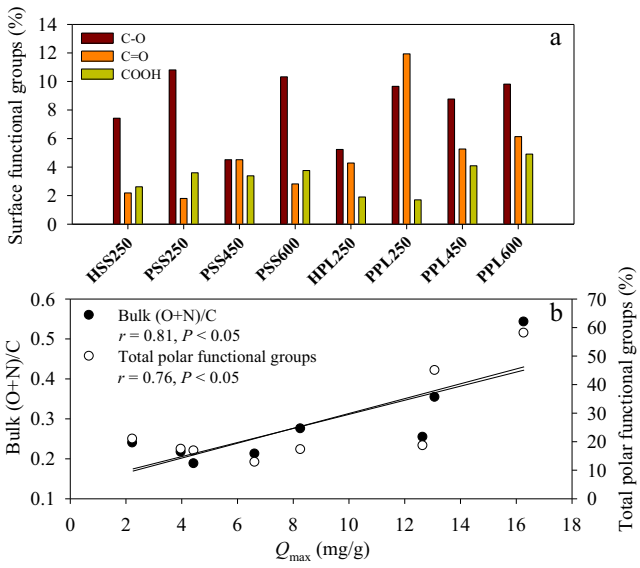

Fig. 1. The percentage (%) of surface C—O, C=O and COOH to total surface carbon-containing functional groups of hydrochars and pyrochars (a); relationship between the bulk (O + N)/C and total functional groups (%) of hydrochars and pyrochars and their maximum adsorption capacity (Q_{max}) of Sb (III) (b).

3.3. Effect of pH on Cd (II) and Sb (III) adsorption

The effects of pH on the adsorption of Cd (II) and Sb (III) by the pyrochars and hydrochars were examined (Fig. 2c and d). All experiments were conducted at pH values (3–6) below the onset of metal hydrolysis and precipitation, estimated as pH > 7.8 for $Cd(OH)_2$. The results indicated that the adsorption of Cd (II) by all the hydrochars and pyrochars generally rose with the increase of pH from 3.0 to 6.0 (Fig. 2c), which was in line with the observation by Elaigwu et al. (2013). Over the studied pH range, the

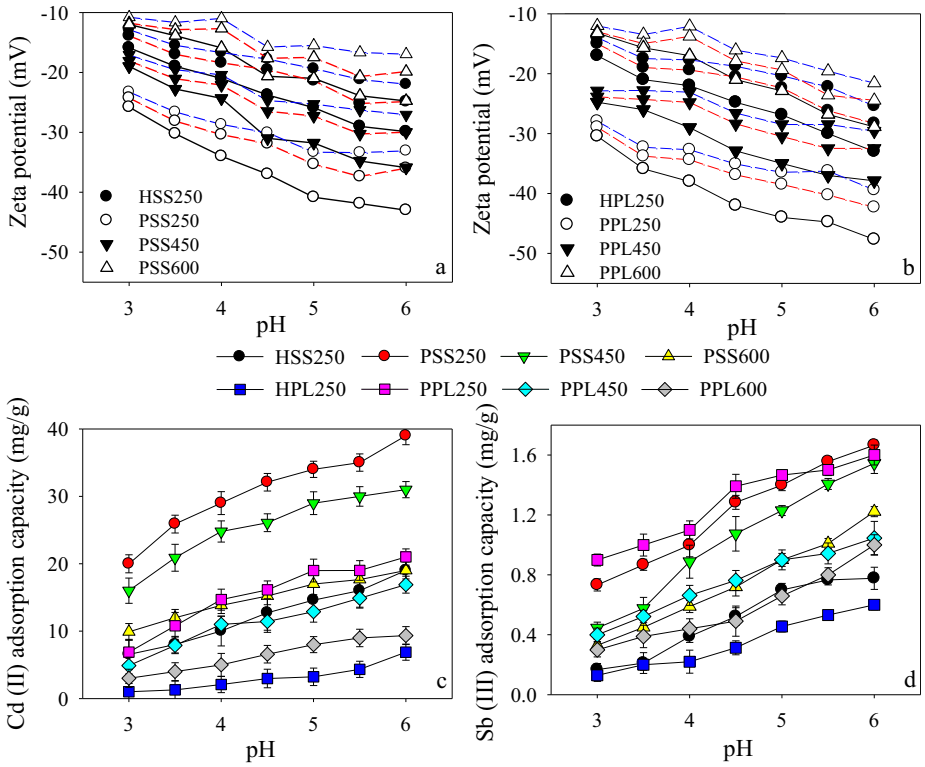

Fig. 2. Zeta potential of hydrochars and pyrochars before and after Cd (II) and Sb (III) adsorption; effect of pH on adsorption of Cd (II) and Sb (III) by hydrochars and pyrochars.

PSS250 showed the highest adsorption capacity for Cd (II), and HPL250 had the lowest adsorption capacity. The following two possible mechanisms could be used to explain the sorption efficiency of hydrochars and pyrochars for Cd (II) as a function of pH. Firstly, the zeta potentials of biochars were all negative and became more negative with the increase of suspension pH (Fig. 2a and b), indicating that the hydrochars and pyrochars possessed variable negative charges on their surface, and the surface charges became more negative with increasing pH. These negative charges of biochars could interact with Cd (II) through electrostatic attraction, and moreover, the electrostatic adsorption increased with the increase of pH. Furthermore, as discussed in the foregoing section, biochars carried the surface functional groups such as —COOH and —OH. These functional groups could interact with Cd (II) to form surface complexes on biochars. With the rise of solution pH, the dissociation of these organic functional groups increased, and thus the ability to form complexes with Cd (II) rose (Tong et al., 2011). This gave another explanation for the increased uptake of Cd (II) by biochars at higher pH.

Different from Cd (II), Sb (III) has been reported to exist primarily as neutral molecule ($Sb(OH)_3$) over a wide pH range (Thanabalasingam and Pickering, 1990). However, similar to Cd (II), Sb (III) adsorption enhanced slightly with pH until the maximum values of 0.78 and 1.67 mg/g on hydrochars and pyrochars, respectively, were obtained at pH 6 (Fig. 2d). The similar results were also reported for Sb (III)-humic acid (Buschmann and Sigg, 2004) and Sb (III)-hydrous oxidize sorption system (Thanabalasingam and Pickering, 1990). The influence of pH on the sorption of Sb (III) onto biochars may be explained by the complexation mechanism. With the increase of pH from 3.0 to 6.0, a substantial part of the polar functional groups (e.g., —COOH) is deprotonated (Alatalo et al., 2013; Kambo and Dutta, 2015; Özkaya, 2006). Two following complexation mechanisms are proposed to occur: (i) ligand exchange at the Sb center and release of hydroxides (Eq. (4)) and (ii) formation of a negatively charged complex (Eq. (5)) (Buschmann and Sigg, 2004). R mainly represents the benzene ring.

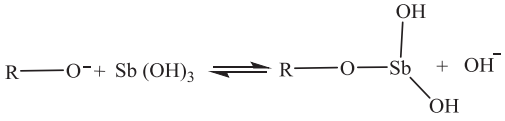

(5)

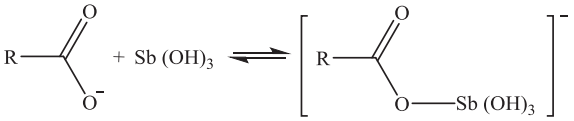

(6)

3.4. Effect of Cd (II) and Sb (III) adsorption on the zeta potential of hydrochars and pyrochars

Previously, it has been documented that electrostatic adsorption of ions by the solid charged-surfaces will not affect the surface charge of particles, since the absorbed ions exist in the diffuse layer of electric double layers on the particles (Xu et al., 2005). By contrast, specific adsorption of ions will be able to change the surface charge and surface potential of solid particles, because these ions can enter the stern layer of electric double layers and form chemical bonds with the solid particle surfaces (Yu, 1997). Considering this, the zeta potential measurements of biochar samples after metal adsorption would give some indication of the contribution of electrostatic adsorption and surface complexation. The results

in Fig. 2a and b clearly illustrated that the presence of Cd (II) and Sb (III) enhanced the zeta potential of biochar particles, demonstrating the occurrence of surface complexation. Additionally, relative to Sb (III), the Cd (II) adsorption induced the higher increase of zeta potential, further suggesting that the surface complexation between biochar and Cd (II) was possibly stronger than that of biochar + Sb (III).

3.5. Effect of Cd (II) and Sb (III) sorption on the FTIR of hydrochars and pyrochars

As aforementioned, Cd (II) and Sb (III) had tendencies to form complexes with functional groups within bicohars. On biochar surfaces, there were various active functional groups (e.g., —COOH, C═O and —OH), which could react with Cd (II) and Sb (III) to form surface complexes, i.e., specific adsorption of Cd (II) and Sb (III) by biochar surfaces. The complexation reactions may result in the variation of chemical environment of some functional groups of biochars (Tong et al., 2011), and thus may lead to a change of their vibrational band in FTIR spectra. Correspondingly, the comparison of FTIR spectra of hydrochars and pyrochars before and after loading Cd (II) and Sb (III) may be conductive to further identifying the functional groups which specially interact with Cd (II) and Sb (III). Figure 3 presents that after adsorption of both Cd (II) and Sb (III), the corresponding peaks of aromatic C═O stretching (~1600 cm^{-1}), and C—O and C═O stretching (~1058 and 1065 cm^{-1}) changed, to some extents. For instance, the peaks of aromatic C═O, and C—O and C═O stretching reduced after loading Cd (II), and moreover, the variation was more significant for swine solid-derived biochars, implying their relatively stronger surface complexation. Additionally, the weaker —OH peak (~3400 cm^{-1}) was observed for poultry litter-based biochars after the treatment with Sb (III). Similar result was reported for a system of pyrochars from soybean stover, in which the interaction of —OH with Sb (III) changed the pyrochars FTIR spectra (Vithanage et al., 2015). These spectra analysis provided the evidence for the formation of surface complexes between Cd (II) and aromatic C═O, C—O and C═O groups within the biochars, and between Sb (III) and aromatic C═O, C—O, C═O and OH groups present on the biochars, respectively.

3.6. Adsorption isotherms of Sb (III) and Cd (II) by pyrochars and hydrochars

3.6.1. Effect of metallic species

The adsorption isotherms of Sb (III) and Cd (II) by all sorbents are shown in Fig. S3. Freundlich, Langmuir and Langmuir-Langmuir equations are classical models for adsorption isotherms of metals. These equations were used to fit adsorption data for the hydrochar and pyrochar systems. A summary of the theoretical parameters and the corresponding R^2 values are listed in Table 2. The R^2 values for the adsorption of Cd (II) and Sb (III) onto the biochars were generally the highest for Langmuir-Langmuir model, demonstrating that Langmuir-Langmuir equation gave the best fit. For all the studied sorbents, the following order was observed for metal ions adsorption: Cd (II) ≫ Sb (III) (Fig. 4a and Table 2). The Q_{max} of hydrochars and pyrochars were 19.80–27.18 and 33.48–81.32 mg/g for Cd (II), and 2.24–3.98 and 4.44–16.28 mg/g for Sb (III), respectively. The higher Q_{max} for Cd (II) than Sb (III) may result from the different metal ion species in aqueous solution. Over the investigated pH range, the Cd (II) was present in the free cationic forms, while Sb (III) was in neutral molecules (Thanabalasingam and Pickering, 1990). Firstly, the neutral Sb $(OH)_3$ less strongly interacted specifically with biochars than positively charged Cd ions, which was confirmed by the less significant rise of zeta potential of biochars after loading Sb (III) than Cd (II) as mentioned in Section 3.3. Additionally, electrostatic adsorption could happen between positively charged Cd and negatively charged biochars, but was negligible between neutral $Sb(OH)_3$ and biochars (Kumar et al., 2011). As a result, compared to Sb (III), relatively more Cd (II) ion could sorb onto the surface of biochars.

3.6.2. Effect of pyrolysis temperature and condition

For a given metal, differences in Q_{max} also existed among hydrochars and pyrochars from different temperatures. For Cd (II) ions, the

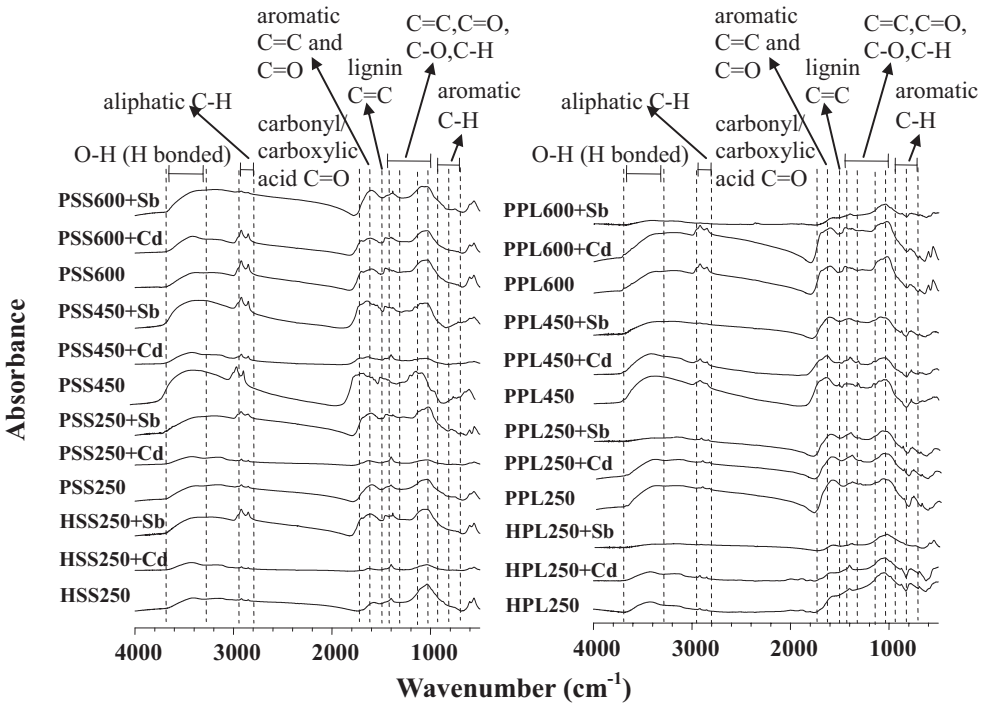

Fig. 3. The FTIR spectra for the hydrochars and pyrochars before and after Cd (II) and Sb (III) adsorption.

Table 2
The sorption parameter for the sorption of Cd (II) and Sb (III).

Samples	F-model[a]			L-model[b]			L-L model[c]					
	K_F	n	R^2	Q_{max}	K_L	R^2	$Q_{max,1}$	K_L	$Q_{max,2}$	K_L	$Q_{max,total}$	R^2
Cd (II)												
HSS250	8.20	0.33	0.960	30.25	0.36	0.980	17.81	0.89	9.38	0.00	27.18	1.000
PSS250	15.01	0.43	0.970	81.12	0.18	0.980	45.61	0.34	35.71	0.02	81.32	0.985
PSS450	3.79	0.62	0.990	79.89	0.05	1.000	37.57	0.06	38.62	0.06	76.18	0.992
PSS600	1.98	0.54	0.990	31.94	0.04	1.000	15.96	0.06	17.48	0.04	33.44	0.993
HPL250	0.90	0.41	0.997	5.43	0.17	0.980	1.56	1.33	18.24	0.00	19.80	0.995
PPL250	4.42	0.52	0.970	55.94	0.06	0.980	27.78	0.07	29.91	0.07	57.69	0.992
PPL450	1.89	0.60	0.980	24.53	0.07	0.970	10.80	0.15	24.35	0.05	35.15	0.971
PPL600	1.01	0.64	0.990	31.16	0.02	0.990	1.79	0.14	31.69	0.01	33.48	0.993
Sb (III)												
HSS250	0.65	0.15	0.997	3.62	0.02	0.999	0.08	1.25	3.90	0.02	3.98	0.999
PSS250	0.60	0.59	1.000	17.12	0.05	0.996	1.89	1.03	11.20	0.02	13.09	1.000
PSS450	0.30	0.74	0.996	11.20	0.02	0.997	12.49	0.01	0.17	0.83	12.66	0.997
PSS600	0.08	0.69	0.995	5.44	0.02	0.999	3.12	0.02	1.33	0.02	4.44	0.999
HPL250	0.13	0.51	0.989	1.41	0.04	0.970	0.19	1.95	2.05	0.01	2.24	0.989
PPL250	0.94	0.50	0.998	8.72	0.10	0.993	7.92	2.89	8.36	0.03	16.28	0.999
PPL450	0.19	0.70	0.998	6.56	0.02	0.998	0.17	2.06	8.11	0.01	8.27	0.999
PPL600	0.05	0.78	0.995	3.57	0.01	0.996	2.73	0.01	3.90	0.08	6.63	0.996

[a] Freundlich model.
[b] Langmuir model.
[c] Langmuir-Langmuir model. Note that the capital "H and P" represent hydrochars and pyrochars, respectively; SS and PL mean the biochars obtained from swine solid and poultry litter, respectively; 250, 450 and 600 refer to the heating treatment temperature (°C) of pyrochars.

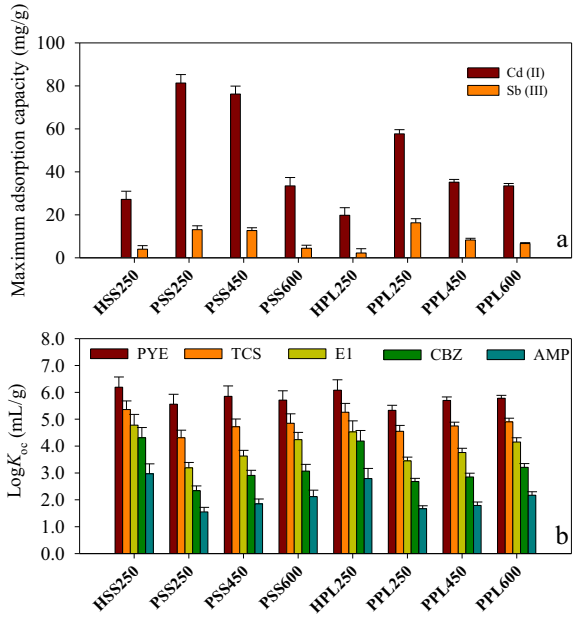

Fig. 4. The maximum sorption capacity (Q_{max}) of Cd (II) and Sb (III) by hydrochars and pyrochars (a); the sorption coefficient ($\log K_{oc}$) of pyrene (PYE), triclosan (TCS), estrone (E1), carbamazepine (CBZ) and acetaminophen (AMP) by hydrochars and pyrochars (b).

Q_{max} of hydrochars and pyrochars derived from swine solids and poultry litter decreased in an order of PSS250 (81.32 mg/g) > PSS450 (76.18 mg/g) > PSS600 (33.44 mg/g) > HSS250 (27.18 mg/g) and PPL250 (57.69 mg/g) > PPL450 (35.15 mg/g) > PPL600 (33.48 mg/g) > HPL250 (19.80 mg/g) (Table 2). The Q_{max} for Sb (III) declined in the same order. Obviously, relative to pyrochars, hydrochars had the lower efficiency in sorbing both Cd (II) and Sb (III), which was in sharp contrast with the high sorption capacity of hydrochars for organic pollutants with a wide range of hydrophobicity (Han et al., 2016; Sun et al., 2011) (Fig. 4b). The lower sorption capacity of hydrochars for Cd (II) and Sb (III) than pyrochars possibly resulted from their low contents of surface functional groups (Fig. 1a) and less negative charges (Fig. 2a and b) (Özkaya, 2006), which was further supported by the positive relationships between the Q_{max} for Sb (III) and bulk polarity and total functional group of all the biochars (Fig. 1b). However, Elaigwu et al. (2013) used microwave-assisted HTC and plant biomass to prepare hydrochar and observed that hydrochar exhibited higher sorption ability for Cd (II) than 350 °C pyrochars. The dissimilar results may be because of the different preparation process of hydrochar. Specific to pyrochars, the Q_{max} for two metals consistently dropped with the increase of HTTs, in line with the change of bulk polarity with HTTs. This phenomenon was also recorded for pyrochars from pecan shell by Uchimiya et al. (2011) and from rice straw by Xu et al. (2014). Additionally, under the same HTT, swine solid-based pyrochars generally showed higher sorption capacity relative to pyrochars from poultry litter. These data pointed out that PSS250 seemed to be good sorbents for the removal of Cd (II) and Sb (III) from aqueous solutions. However, as above-mentioned, PSS250 showed low C stability indexes and SOMYI, indicating that it would not reside in soils for a long period of time. Lehmann and Joseph (2015) underscored that "if biochars could be decomposed rapidly, their valuable benefits would be affected in extent and duration". Thus, PSS250 was not a satisfactory material for sorbing and retaining Cd (II) and Sb (III). Recently, Guo and Chen (2014) reported that OC stability of 500 °C rice straw-based biochar was influenced not only by their aromaticity but also through possible protection by silicon encapsulation, resulting in that OC stability of 500 °C pyrochar was not necessarily lower than that of 700 °C one. Furthermore, on the basis of results by Singh et al. (2012), it could be estimated that OC of 450 °C biochars was comparatively stable, with the mean residence time varying between 90 and 1600 years. Moreover, the data in Table 1 directly illustrated that OC of 450 °C pyrochars were relatively stable, with comparatively high values of OC stability indexes and SOMYI. These, along with the fact that PSS450 had almost similar Q_{max} for Cd (II) and Sb (III) with PSS250, indicated that PSS450 was the better sorbent to immobilize Cd (II) and Sb (III). According to the obtained Q_{max} values for Cd (II) (76.18 mg/g) and Sb (III) (12.66 mg/g) at pH of 4.5, the possible weight ratios of PSS450 to Cd (II) and Sb (III) in practical wastewater treatment could be 13.13 and 78.99, respectively. However, the actual percentage must be determined in the consideration of prac-

Table 3
Adsorption capacities of different biochars for Cd (II) and Sb (III).

Adsorbents	Sorption capacity (mg/g)		References
	Cd (II)	Sb (III)	
Hydrochars			
200 °C hydrochar from *Prosopis africana* shell	38.30	–	Elaigwu et al. (2013)
200 °C hydrochar from sawdust	40.78		Sun et al. (2015)
200 °C hydrochar from wheat straw	38.75		Sun et al. (2015)
200 °C hydrochar from corn stalk	30.40		Sun et al. (2015)
250 °C hydrochar from swine solids	27.18	3.98	This study
250 °C hydrochar from poultry litter	19.80	2.24	This study
Pyrochars			
Plant-derived pyrochars			
350 °C pyrochar from *Prosopis africana* shell	29.90	–	Elaigwu et al. (2013)
200 °C pyrochar from *Ceiba pentandra* hull	19.60		Rao et al. (2006)
450 °C pyrochar from rice straw	3.03		Xu et al. (2014)
600 °C pyrochar from rice straw	3.83		Xu et al. (2014)
450 °C pyrochar from wheat straw	5.00		Xu et al. (2014)
600 °C pyrochar from wheat straw	1.96		Xu et al. (2014)
450 °C pyrochar from oak wood	0.37		Mohan et al. (2013)
450 °C pyrochar from pine bark	0.34		Mohan et al. (2013)
450 °C pyrochar from oak bark	5.40		Mohan et al. (2013)
700 °C pyrochar from buffalo weed	11.33		Titirici et al. (2012)
400 °C pyrochar from rice straw	34.13		Mohan et al. (2013)
300 °C pyrochar from soybean stover		4.63	Vithanage et al. (2015)
Animal manure-derived pyrochars			
300 °C pyrochar from swine solid	42.44		Xu et al. (2014)
450 °C pyrochar from swine solid	52.45		Xu et al. (2014)
600 °C pyrochar from swine solid	22.68		Xu et al. (2014)
200 °C pyrochar from dairy manure	32.02		Sun et al. (2013)
350 °C pyrochar from dairy manure	54.63		Sun et al. (2013)
400 °C pyrochar from pig manure	107.08		Filella et al. (2002a)
600 °C pyrochar from pig manure	117.01		Filella et al. (2002a)
400 °C pyrochar from cow manure	114.75		Filella et al. (2002a)
400 °C pyrochar from cow manure	118.40		Filella et al. (2002a)
400 °C pyrochar from cow manure	78.19		Filella et al. (2002a)
600 °C pyrochar from cow manure	82.30		Filella et al. (2002a)
250 °C pyrochar from swine solid	81.32	13.09	This study
450 °C pyrochar from swine solid	76.18	12.66	This study
600 °C pyrochar from swine solid	33.44	4.44	This study
250 °C pyrochar from poultry litter	57.69	16.28	This study
450 °C pyrochar from poultry litter	35.15	8.27	This study
600 °C pyrochar from poultry litter	33.48	6.63	This study

tical solution conditions (e.g., pH, salinity and temperature) of wastewaters.

The sorption capacities of other biochars for Cd (II) and Sb (III) in the literature were also cited in this study (Table 3). It was noticed that the adsorption capacities of pyrochars for Cd (II) in this study (33.44–81.32 mg/g) were comparable with manure-derived pyrochars (22.68–118.40 mg/g) in previous studies (Filella et al., 2002a; Sun et al., 2013; Tong et al., 2011), but significantly higher than plant-derived hydrochars (30.40–40.78 mg/g) and pyrochars (0.34–34.13 mg/g) (Audry et al., 2004; Buschmann and Sigg, 2004; Mohan et al., 2013; Sundar and Chakravarty, 2010; Titirici et al., 2012) (Table 3). The higher ash content of manure-derived pyrochar than plant-derived one may account for its higher sorption affinity for metals (Mohan et al., 2014). Exchange between cations the ash of manure-derived pyrochars and Cd (II) was possibly the main potential mechanism. It could be seen that besides C, N, and O, calcium (Ca), silicon (Si) and phosphorus (P) were also detected on the surface of the studied manure-derived biochars (Table 1). Ca on the surface of biochars may be mainly the calcium carbonate or calcium phosphates. Because the Cd (II) adsorption was conducted under the acidic environment, these complexes or/and precipitates on biochars might be dissociated or dissolved, and then the new adsorption sites could be provided via the exchange of Ca (II) with Cd (II) (Xu et al., 2014). Moreover, it was noted that although hydrochars exhibited the lower effectiveness in removing Cd (II) than manure-pyrochars, they had higher sorption capacities for Cd (II) than most of plant-based pyrochars. Moreover, Table 3 clearly and directly illustrated that Sb sorption onto biochars was not widely studied, making the comparison of sorption potential for Sb (III) challenging. One research group has studied the Sb (III) removal by 300 °C pyrochars from soybean stover (Vithanage et al., 2015). Removal efficiency towards Sb (III) was 4.63 mg/g, similar to that of hydrochars (2.24–3.98 mg/g) but lower than that of pyrochars (4.44–16.28 mg/g) in this work. In view of the limited studies on the Sb (III) sorption by biochars, its sorption values by other carbon sorbents (e.g., biomass, activated carbon) were also cited to make a further comparison (Iqbal et al., 2013; Koshima and Onishi, 1985; Wang et al., 2012). It was found that the Q_{max} values (12.66–16.28 mg/g) of 250 °C pyrochars and PSS450 in this study were comparable with or slightly lower than those of bean husk (20.14 mg/g) reported by Iqbal et al. (2013) and activated carbon (15–24 mg/g) by Koshima and Onishi (1985), but much higher than those of activated carbon (2.13–4.81 mg/g) by Wang et al. (2012).

4. Conclusions

Cd (II) adsorption onto hydrochar and pyrochars was demonstrated to occur through both specific and electrostatic mechanisms, and Sb (III) mainly interacted with hydrochar and pyrochars through surface complexation. Relative to hydrochars from both plant and manure, manure-based pyrochars showed higher sorption capacity. Among six manure-based pyrochars, 450 °C swine solid-derived pyrochar was identified to be more

suitable to immobilize Cd (II) and Sb (III). However, it should be mentioned that its sorption efficiency might be inhibited in strongly acidic wastewater. In future studies, detailed effect of process parameters (e.g., salinity and temperature) on the sorption should be addressed.

Acknowledgements

The authors would like to acknowledge the technical support provided by Mr. Melvin Johnson of the USDA-ARS Coastal Plains Soil, Water & Plant Research Center, Florence, SC. This research was supported by the National Natural Science Foundation--Outstanding Youth Foundation (41522303), the National Natural Science Foundation of China (41473087), State Education Ministry, and USDA McIntire-Stennis Program (MAS 00028). L. Han also thanks the China Scholarship Council for supporting her study at the University of Massachusetts, Amherst. Mention of trade names or commercial products is solely for the purpose of providing specific information and does not imply recommendation or endorsement by the U.S. Department of Agriculture.

Appendix A. Supplementary material

Supplementary data associated with this article can be found, in the online version, at http://dx.doi.org/10.1016/j.biortech.2017.02.130.

References

Alatalo, S.M., Repo, E., Mäkilä, E., Salonen, J., Vakkilainen, E., Sillanpää, M., 2013. Adsorption behavior of hydrothermally treated municipal sludge & pulp and paper industry sludge. Bioresour. Technol. 147, 71–76.

Audry, S., Schäfer, J., Blanc, G., Jouanneau, J.M., 2004. Fifty-year sedimentary record of heavy metal pollution (Cd, Zn, Cu, Pb) in the Lot River reservoirs (France). Environ. Pollut. 132 (3), 413–426.

Berge, N.D., Ro, K.S., Mao, J., Flora, J.R., Chappell, M.A., Bae, S., 2011. Hydrothermal carbonization of municipal waste streams. Environ. Sci. Technol. 45 (13), 5696–5703.

Buschmann, J., Sigg, L., 2004. Antimony (III) binding to humic substances: influence of pH and type of humic acid. Environ. Sci. Technol. 38 (17), 4535–4541.

Cao, X., Ro, K.S., Libra, J.A., Kammann, C.I., Lima, I., Berge, N., Li, L., Li, Y., Chen, N., Yang, J., 2013. Effects of biomass types and carbonization conditions on the chemical characteristics of hydrochars. J. Agric. Food Chem. 61 (39), 9401–9411.

Crombie, K., Mašek, O., Sohi, S.P., Brownsort, P., Cross, A., 2013. The effect of pyrolysis conditions on biochar stability as determined by three methods. GCB Bioenergy 5 (2), 122–131.

D1762-84, 2007. Standard Test Method for Chemical Analysis of Wood Charcoal. American Society for Testing and Materials (ASTM), Conshohocken, PA.

Elaigwu, S.E., Rocher, V., Kyriakou, G., Greenway, G.M., 2013. Removal of Pb^{2+} and Cd^{2+} from aqueous solution using chars from pyrolysis and microwave-assisted hydrothermal carbonization of *Prosopis africana* shell. J. Ind. Eng. Chem. 20 (5), 3467–3473.

Filella, M., Belzile, N., Chen, Y.W., 2002a. Antimony in the environment: a review focused on natural waters: I. Occurrence. Earth-Sci. Rev. 57 (1–2), 125–176.

Filella, M., Belzile, N., Chen, Y.W., 2002b. Antimony in the environment: a review focused on natural waters: II. Relevant solution chemistry. Earth-Sci. Rev. 59 (1), 265–285.

Guo, J., Chen, B., 2014. Insights on the molecular mechanism for the recalcitrance of biochars: interactive effects of carbon and silicon components. Environ. Sci. Technol. 48 (16), 9103–9112.

Han, L., Ro, K.S., Sun, K., Jin, J., Libra, J.A., Xing, B., 2016. New evidence for high sorption capacity of hydrochar for hydrophobic organic pollutants. Environ. Sci. Technol. 50 (24), 13274–13282.

Iqbal, M., Saeed, A., Edyvean, R.G.J., 2013. Bioremoval of antimony (III) from contaminated water using several plant wastes: optimization of batch and dynamic flow conditions for sorption by green bean husk (*Vigna radiata*). Chem. Eng. J. 225, 192–201.

Järup, L., 2003. Hazards of heavy metal contamination. Br. Med. Bull. 68 (486), 167–182.

Kambo, H.S., Dutta, A., 2015. A comparative review of biochar and hydrochar in terms of production, physico-chemical properties and applications. Renew. Sust. Energy Rev. 45, 359–378.

Koshima, H., Onishi, H., 1985. Adsorption of iron (III), gallium (III), thallium (III), antimony (V) and antimony (III) on activated carbon from hydrochloric acid solution. Anal. Sci. 1 (3), 237–240.

Kumar, S., Loganathan, V.A., Gupta, R.B., Barnett, M.O., 2011. An assessment of U (VI) removal from groundwater using biochar produced from hydrothermal carbonization. J. Environ. Manage. 92 (10), 2504–2512.

Lehmann, J., Joseph, S., 2015. Biochar for Environmental Management: Science, Technology and Implementation. Routledge.

Leuz, A.K., Mönch, H., Johnson, C.A., 2006. Sorption of Sb (III) and Sb (V) to goethite: influence on Sb (III) oxidation and mobilization. Environ. Sci. Technol. 40 (23), 7277–7282.

Libra, J.A., Ro, K.S., Kammann, C., Funke, A., Berge, N.D., Neubauer, Y., Titirici, M.M., Fühner, C., Bens, O., Kern, J., 2011. Hydrothermal carbonization of biomass residuals: a comparative review of the chemistry, processes and applications of wet and dry pyrolysis. Biofuels 2 (1), 71–106.

Masto, R.E., Kumar, S., Rout, T.K., Sarkar, P., George, J., Ram, L.C., 2013. Biochar from water hyacinth (*Eichornia crassipes*) and its impact on soil biological activity. Catena 111, 64–71.

Mohan, D., Kumar, H., Sarswat, A., Alexandre-Franco, M., Pittman, C.U., 2013. Cadmium and lead remediation using magnetic oak wood and oak bark fast pyrolysis biochars. Chem. Eng. J. 236 (2), 513–528.

Mohan, D., Sarswat, A., Ok, Y.S., Pittman, C.U., 2014. Organic and inorganic contaminants removal from water with biochar, a renewable, low cost and sustainable adsorbent-a critical review. Bioresour. Technol. 160, 191–202.

Mumme, J., Eckervogt, L., Pielert, J., Diakité, M., Rupp, F., Kern, J., 2011. Hydrothermal carbonization of anaerobically digested maize silage. Bioresour. Technol. 102 (19), 9255–9260.

Özkaya, B., 2006. Adsorption and desorption of phenol on activated carbon and a comparison of isotherm models. J. Hazard. Mater. 129 (1), 158–163.

Qiu, M., Sun, K., Jin, J., Gao, B., Yan, Y., Han, L., Wu, F., Xing, B., 2014. Properties of the plant-and manure-derived biochars and their sorption of dibutyl phthalate and phenanthrene. Sci. Rep. 4.

Ran, Y., Sun, K., Yang, Y., Xing, B., Zeng, E., 2007. Strong sorption of phenanthrene by condensed organic matter in soils and sediments. Environ. Sci. Technol. 41 (11), 3952–3958.

Rao, M.M., Ramesh, A., Rao, G.P.C., Seshaiah, K., 2006. Removal of copper and cadmium from the aqueous solutions by activated carbon derived from *Ceiba pentandra* hulls. J. Hazard. Mater. 129 (1–3), 123–129.

Singh, B.P., Cowie, A.L., Smernik, R.J., 2012. Biochar carbon stability in a clayey soil as a function of feedstock and pyrolysis temperature. Environ. Sci. Technol. 46 (21), 11770–11778.

Spokas, K.A., Novak, J.M., Stewart, C.E., Cantrell, K.B., Uchimiya, M., DuSaire, M.G., Ro, K.S., 2011. Qualitative analysis of volatile organic compounds on biochar. Chemosphere 85 (5), 869–882.

Sun, K., Kang, M., Zhang, Z., Jin, J., Wang, Z., Pan, Z., Xu, D., Wu, F., Xing, B., 2013. Impact of deashing treatment on biochar structural properties and potential sorption mechanisms of phenanthrene. Environ. Sci. Technol. 47 (20), 11473–11481.

Sun, K., Ro, K., Guo, M., Novak, J., Mashayekhi, H., Xing, B., 2011. Sorption of bisphenol A, 17α-ethinyl estradiol and phenanthrene on thermally and hydrothermally produced biochars. Bioresour. Technol. 102 (10), 5757–5763.

Sun, K., Tang, J., Gong, Y., Zhang, H., 2015. Characterization of potassium hydroxide (KOH) modified hydrochars from different feedstocks for enhanced removal of heavy metals from water. Environ. Sci. Pollut. Res. 22 (21), 1–12.

Sundar, S., Chakravarty, J., 2010. Antimony toxicity. Int. J. Environ. Res. Public Health 7 (12), 4267–4277.

Thanabalasingam, P., Pickering, W., 1990. Specific sorption of antimony (III) by the hydrous oxides of Mn, Fe, and Al. Water Air Soil Pollut. 49 (1–2), 175–185.

Titirici, M.M., White, R.J., Falco, C., Sevilla, M., 2012. Black perspectives for a green future: hydrothermal carbons for environment protection and energy storage. Energy Environ. Sci. 5 (5), 6796–6822.

Tong, X.J., Li, J.Y., Yuan, J.H., Xu, R.K., 2011. Adsorption of Cu (II) by biochars generated from three crop straws. Chem. Eng. J. 172 (2–3), 828–834.

Uchimiya, M., Klasson, K.T., Wartelle, L.H., Lima, I.M., 2011. Influence of soil properties on heavy metal sequestration by biochar amendment: 1. Copper sorption isotherms and the release of cations. Chemosphere 82 (10), 1431–1437.

Uchimiya, M., Lima, I.M., Thomas, K.K., Chang, S., Wartelle, L.H., Rodgers, J.E., 2010. Immobilization of heavy metal ions (Cu^{II}, Cd^{II}, Ni^{II}, and Pb^{II}) by broiler litter-derived biochars in water and soil. J. Agric. Food Chem. 58 (9), 5538–5544.

Vithanage, M., Rajapaksha, A.U., Ahmad, M., Uchimiya, M., Dou, X., Alessi, D.S., Ok, Y. S., 2015. Mechanisms of antimony adsorption onto soybean stover-derived biochar in aqueous solutions. J. Environ. Manage. 151, 443–449.

Waalkes, M.P., 2000. Cadmium carcinogenesis in review. J. Inorg. Biochem. 79 (1), 241–244.

Wang, X.H., Yu, T.C., Li, C., Ye, M.M., 2012. The adsorption of Sb (III) in aqueous by $KMnO_4$-modified activated carbon. J. Zhejiang Univ. (Eng. Sci.) 11, 017.

Xu, D., Ye, Z., Ke, S., Bo, G., Wang, Z., Jie, J., Zhang, Z., Wang, S., Yu, Y., Liu, X., 2014. Cadmium adsorption on plant- and manure-derived biochar and biochar-amended sandy soils: impact of bulk and surface properties. Chemosphere 111C, 320–326.

Xu, R., Xiao, S., Zhao, A., Ji, G., 2005. Effect of Cr (VI) anions on adsorption and desorption behavior of Cu (II) in the colloidal systems of two authentic variable charge soils. J. Colloid Interf. Sci. 284 (1), 22–29.

Xu, X., Cao, X., Zhao, L., Wang, H., Yu, H., Gao, B., 2013. Removal of Cu, Zn, and Cd from aqueous solutions by the dairy manure-derived biochar. Environ. Sci. Pollut. Res. 20 (1), 358–368.

Yu, T., 1997. Chemistry of Variable Charge Soils. Oxford University Press, New York.